

## Colloidal Cutin-Like Substances Cross-Linked to Siderophore Decomposition Products Mobilizing Plutonium from Contaminated Soils

C. XU,<sup>†</sup> P.H. SANTSCHI,<sup>\*,†</sup> J.Y. ZHONG,<sup>‡</sup> P.G. HATCHER,<sup>‡</sup> A.J. FRANCIS,<sup>§</sup> C.J. DODGE,<sup>§</sup> K.A. ROBERTS,<sup>†</sup> C.-C. HUNG,<sup>||</sup> AND B.D. HONEYMAN<sup>⊥</sup>

Laboratory for Oceanographic and Environmental Research (LOER), Departments of Oceanography and Marine Sciences, Texas A&M University, Galveston, Texas 77551, COSMIC Laboratory, College of Sciences, Old Dominion University, Norfolk, Virginia 23529, Environmental Sciences Department, Brookhaven National Laboratory, Upton, New York 11973, Institute of Marine Environmental Chemistry and Ecology, National Taiwan Ocean University, 2 Pei-Ning Rd, Keelung, 202, Taiwan, and Laboratory for Applied and Environmental Radiochemistry, Environmental Science and Engineering Division, Colorado School of Mines, Golden, Colorado 80401

Received May 15, 2008. Revised manuscript received August 19, 2008. Accepted September 2, 2008.

Relatively recently, inorganic colloids have been invoked to reconcile the apparent contradictions between expectations based on classical dissolved-phase Pu transport and field observations of "enhanced" Pu mobility (Kersting et al. *Nature* **1999**, *397*, 56–59). A new paradigm for Pu transport is mobilization and transport via biologically produced ligands. This study for the first time reports a new finding of Pu being transported, at sub-pM concentrations, by a cutin-like natural substance containing siderophore-like moieties and virtually all mobile Pu. Most likely, Pu is complexed by chelating groups derived from siderophores that are covalently bound to a backbone of cutin-derived soil degradation products, thus revealing the history of initial exposure to Pu. Features such as amphiphilicity and small size make this macromolecule an ideal collector for actinides and other metals and a vector for their dispersal. Cross-linking to the hydrophobic domains (e.g., by polysaccharides) gives this macromolecule high mobility and a means of enhancing Pu transport. This finding provides a new mechanism for Pu transport through environmental systems that would not have been predicted by Pu transport models.

### Introduction

Plutonium's low solubility and high particle reactivity led to the conventional wisdom that it is essentially immobile in the subsurface environment. Classically, Pu distribution

throughout the environment has been considered to be primarily the consequence of wind and water erosion of particles from surficial soils and sediments. Confounding this expectation are observations of Pu concentrations approaching or exceeding the drinking water limit of  $10^{-12}$  M at substantial distances from known source zones (2). It has recently been shown that colloids rich in Al-silicates (1), organic carbon (3), or iron (4) are capable of facilitating transport of Pu from contaminated sites, possibly over distances of many kilometers. Under most surface soil conditions, and with few exceptions (5, 6), +4 is the dominant Pu oxidation state (7); a state that has the ability to form complexes with a range of environmental ligands (e.g., metal oxides, organic macromolecules, cell walls) (7, 8). However, few studies (3) have shown that the mobile environmental form of Pu is Pu-organic ligand complexes.

The Rocky Flats Nuclear Weapons Plant manufactured components for nuclear weapons for the Nation's defense until 1989. Surficial soils at RFETS contain elevated  $^{239,240}\text{Pu}$  concentrations due to soil contamination in the 1960s from leaking drums stored on the 903 Pad area whereby Pu-contaminated soil particles were later dispersed by wind and water. Although environmental remediation activities were completed in 2006, residual Pu remains in grassland soils of the site (9). Field studies of storm runoff and pond discharge samples from this site (3), collected before remediation, demonstrated that off-site transport of the  $^{239,240}\text{Pu}$  occurred in the particulate ( $\geq 0.45 \mu\text{m}$ ; 40–90%) and colloidal ( $\sim 2 \text{ nm}$  or 3 kDa to  $0.45 \mu\text{m}$ ; 10–60%) size classes, amounting to an annual flux, estimated from flow and concentration data, of about 1–10  $\mu\text{Ci}$  of Pu away from the site. Controlled laboratory experiments (3) further confirmed that  $\geq 80\%$  of dissolved Pu ( $< 0.45 \mu\text{m}$ ) in surface waters was present in the colloidal phase. Most importantly, isoelectric focusing (IEF) experiments conducted with this aqueous leachate material revealed that colloidal Pu, in the tetra-valent (IV) state, as determined by analogy to Th(IV) (3), was mostly associated with a negatively charged iron-containing organic macromolecule with an isoelectric point ( $\text{pH}_{\text{IEF}}$ ) of 3.1 and a molecular weight of 6 kDa, rather than with inorganic (e.g., aluminosilicates) colloids. However, previous studies lacked the molecular level characterization needed to elucidate the composition and structure of this Pu-enriched colloidal organic carrier. This study fully describes for the first time an amphiphilic, organic colloidal class of compounds that contains much higher Pu concentration than either the ambient soil or bulk colloid, and can be easily leached out from the natural soil by rainwater in vadose and saturated zones as well as waste stream areas. This finding is of great environmental implication since it reveals one of the possible pathways how "man-made" Pu can become mobile, and transported long distance.

### Experimental Section

**Sample Collection.** The RFETS soil was collected in 2004 from the upper 15 cm at a grass-covered hill slope, in the drainage of the neighboring creeks (Figure S1 in the Supporting Information (SI)). Details of the soil information are provided in SI Table S1. Sieved soil ( $< 1 \text{ mm}$ ) was resuspended to a point of equilibrium in filtered tap water ( $< 0.45 \mu\text{m}$ ) overnight to (1) simulate the release of mobile colloidal matter by storm and erosion events, and (2) protect the structure and conformation of water-dispersible colloids from any traditional harsh chemical treatment. A mobile colloidal fraction (3 kDa– $0.45 \mu\text{m}$ ) was obtained from this slurry by

\* Corresponding author phone: +1 409 7404476; fax: +1 409 7404786; e-mail: santschi@tamug.edu.

<sup>†</sup> Texas A&M University.

<sup>‡</sup> Old Dominion University.

<sup>§</sup> Brookhaven National Laboratory.

<sup>||</sup> National Taiwan Ocean University.

<sup>⊥</sup> Colorado School of Mines.

**TABLE 1. Comparison of Chemical Composition of RFETS Soil, Water Extract, and IEF Extract<sup>a</sup>**

|               | yield<br>mg/kg | Pu<br>(pCi/g) | OC<br>(%,wt) | N/C atom<br>ratio | C-AHA/C<br>atom ratio | TCHO-C<br>(%, OC) | protein-C<br>(%, OC) | URA-C<br>(%, OC) | PO <sub>4</sub> <sup>3-</sup> /C mol<br>ratio (× 10 <sup>-4</sup> ) | SO <sub>4</sub> <sup>2-</sup> /C mol<br>ratio (× 10 <sup>-4</sup> ) | Fe/C mol<br>ratio (× 10 <sup>-2</sup> ) | Mn/C mol<br>ratio (× 10 <sup>-4</sup> ) | Al/C mol<br>ratio (× 10 <sup>-2</sup> ) | size            |
|---------------|----------------|---------------|--------------|-------------------|-----------------------|-------------------|----------------------|------------------|---|---|---|---|---|-----------------|
| original soil | ~1             | 351 ± 7       | 2.0 ± 0.3    | 0.050 ± 0.013     | 0.005                 | 17.9 ± 0.8        | 15.9 ± 2.9           | 7.2 ± 0.9        | 0.68 ± 0.07   | 28.0 ± 4.1  | 30.30 ± 0.68                            | 43.6 ± 4.3                              | 92.07 ± 4.39                            | ≤ 1 mm          |
| water extract | 383            | 660 ± 47      | 28.6 ± 0.8   | 0.063 ± 0.026     | ND                    | 11.5 ± 1.0        | 7.4                  | 1.3 ± 0.2        | 0.13 ± 0.01   | 548.7 ± 1.5   | 0.02 ± 0.00                             | 3.81 ± 0.95                             | 0.18                                    | 2–450 nm        |
| IEF extract   | 114            | 3222 ± 278    | 48.8 ± 0.3   | 0.203 ± 0.037     | 0.01                  | 4.7 ± 1.6         | 1.9 ± 0.7            | 0.4 ± 0.1        | 0.01 ± 0.00   | 139.7 ± 32.1  | 0.05 ± 0.03                             | 0.09 ± 0.03                             | 0.15 ± 0.01                             | (5.9 ± 0.7) kDa |

<sup>a</sup> Errors are 1 standard deviation from replicate determinations of samples; activity concentrations of Pu in pCi/g, with 27 pCi = 1 Bq; OC (%), percentage of organic carbon in total mass; C-AHA/C atom ratio: atom ratio of carbon in the hydroxamic acid (AHA) functional group (–CO–N(OH)–) to total organic carbon in sample; TCHO-C (%), percentage of total carbohydrates-C (40%) in total organic carbon; Protein-C (%), percentage of protein-C (analyzed as total protein, and assumed to contain 33% C) in total organic carbon; URA-C (%), percentage of uronic acid-C (37.11%) in total organic carbon. All other elements, i.e., N, PO<sub>4</sub><sup>3-</sup>, SO<sub>4</sub><sup>2-</sup>, Fe, Mn, Al, were converted into atom ratio to carbon; ND, not determined.

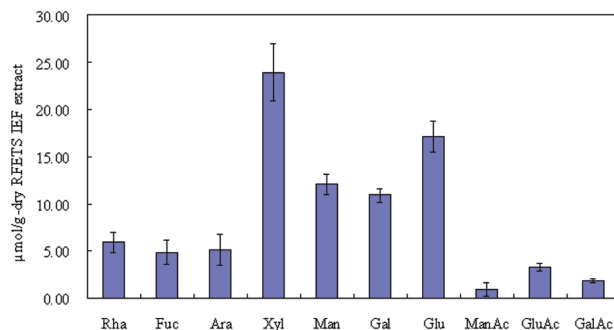


**FIGURE 1. Individual monosaccharides of RFETS soil colloidal IEF extract.**

resuspension, followed by filtration and diafiltration (Figure S2). This colloidal material, containing ambient <sup>239,240</sup>Pu and to which <sup>234</sup>Th was added as a proxy tracer, was called the “water extract” and was subsequently fractionated using isoelectric focusing gel electrophoresis. The low pH isolate (0–1 cm of the IEF gel), where both actinides were the most enriched (Figure S3), was extracted from the gel with 1% SDS and then diafiltered against nanopure water through a 3 kDa regenerated cellulose membrane in an Amicon stirred cell series 8400 (Millipore Corporation) to remove all the electrophoresis reagents. The retentate was freeze-dried and prepared for further characterization. To obtain sufficient material for molecular level analysis (e.g., NMR), the IEF focusing was conducted numerous times and the sections of IEF gel which were enriched in Pu activity were pooled. This isolate was called the “IEF extract”. IEF blank gels were treated the same way as sample gels through all extraction, diafiltration, and freeze-drying steps and confirmed that contamination from the reagents (ampholytes, rehydration solutions, extractants, etc.) and the gel material was negligible.

**Analysis.** Characterization included the spectrophotometric analysis of total carbohydrates, uronic acids (10), proteins (11), and phosphate (12); elemental analysis of organic C and N by Perkin-Elmer CHNS 2400 analyzer (13); determination of Fe, Al, and Mn by Perkin-Elmer 5100 Zeeman GFAAS (3); and measurement of sulfate by ion chromatography (Dionex, Houston, TX) with an IonPac AG4A anion guard and analytical columns, after an acid hydrolysis step (14). For the IEF extract, the molecular weight was determined by using a Tosoh Biosciences G4000 PWxl guard and analytical size exclusion columns coupled with a Waters HPLC system. Polysulfonate standards were used for calibration (see SI). Hydrolyzable sugar composition was determined by a Thermo-Finnigan GC-EI-MS after derivatization (15). Functional groups were identified by a Varian 3100 FTIR, connected with a single reflection horizontal ATR accessory from PIKE Technologies, Inc. (Madison, WI).

Solid-state DPMAS <sup>13</sup>C, <sup>15</sup>N NMR, and 1D <sup>1</sup>H, 2D-HRMAS-NMR (HSQC and COSY) of the IEF extract were acquired on a Bruker Avance II 400 MHz NMR-spectrometer (Bruker-Biospin, Billerica, MA) at ODU. Spectra were obtained using Topspin 2.0 software distributed by Bruker-Biospin. Spectral simulations were carried out using Advanced Chemistry Development’s (ACD/Laboratories) Spec Manager (version 9.15) software.

For both the water and IEF extracts, microsynchrotron X-ray fluorescence (SXRF) was performed to determine the elemental distribution of Fe, Mn, Ca, and Ti in both the water and IEF extracts. Micro-X-ray absorption ( $\mu$ -XANES) near edge spectroscopy analysis was performed at BNL at the Fe and Mn K edges to obtain oxidation state information.

## Results and Discussion

**Chemical Composition.** Figure S3 presents the result of an IEF run carried out with a <sup>234</sup>Th spiked RFETS soil–water

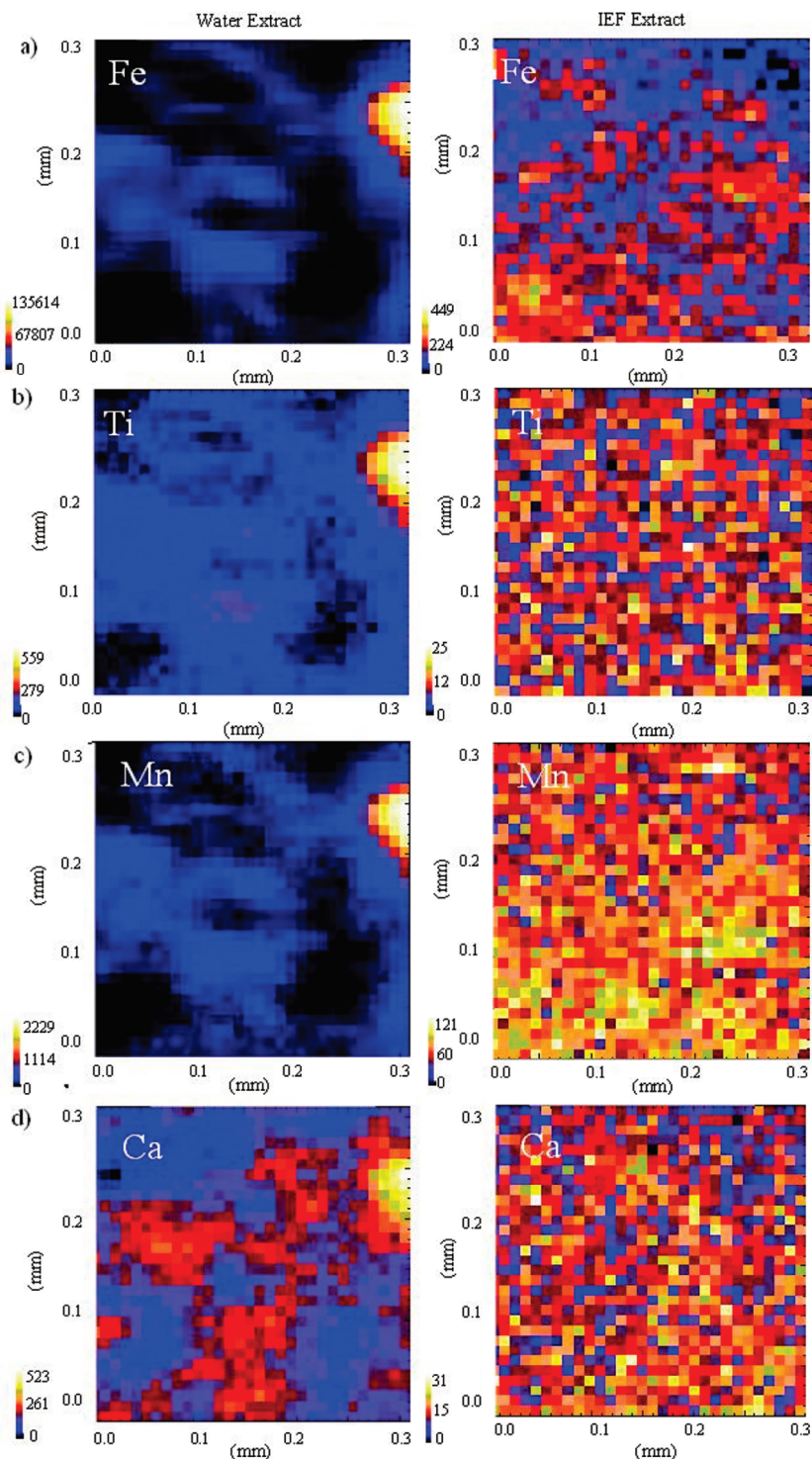


**FIGURE 2.** Synchrotron-based  $\mu$ -X-ray fluorescence map of Fe (a), Ti (b), Mn (c), and Ca (d) in Rocky Flats colloids. Left, water extract; right, IEF extract. The relative concentration of each metal in the map is given in the ascending color scale at the bottom left of the figure. The intensity maps have not been calibrated so an estimate of metal concentrations in the colloid was not obtained. Each pixel is  $10\ \mu\text{m} \times 10\ \mu\text{m}$ .

extract, having a specific activity of  $^{239,240}\text{Pu}$  of  $660 \pm 47\ \text{pCi/g}$ . It was found that  $^{234}\text{Th}$  (IV) tracked the  $^{239,240}\text{Pu}$  activity fairly well, with a significant peak for both radionuclides at a pH of 3 near the beginning of the gel (0–1 cm), indicating a low isoelectric point and negative charge at neutral pH for the carrier molecules. This suggests that both actinides likely have a complexation behavior similar to that of specific clustered functional groups of organic matter (16). Recoveries of both isotopes ( $^{234}\text{Th}$  (IV) and  $^{239,240}\text{Pu}$  (IV)), calculated as the sum of activity over all gel fractions normalized to the

total activity used in IEF, were  $83 (\pm 4)\%$  and  $66 (\pm 5)\%$ , respectively, with the remainder adsorbed onto the container walls. The specific activity of Pu is about an order of magnitude greater in the IEF extract than in the bulk soil. Mass balance calculations also indicate that the colloidal Pu is, for the most part, contained in this IEF extract (pH = 3). The amounts of Pu and OC that can be measured in this water extract (i.e., 0.1% of the total Pu and 0.6% of the total OC in the bulk soil) are similar to those that were reported previously (3) for the less vegetated soil case. Furthermore,

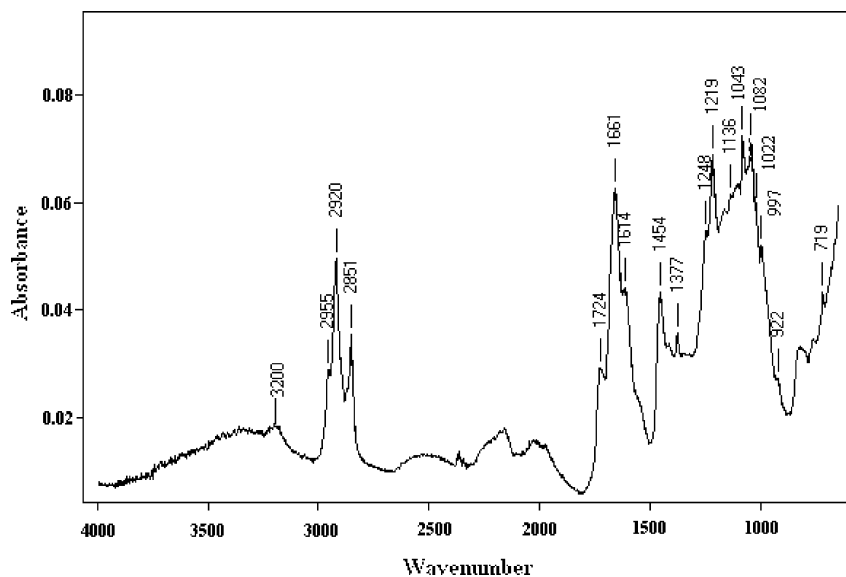


FIGURE 3. ATR-FTIR spectrum of RFETS soil IEF extract.

the mole ratio of Fe to OC of  $2 \times 10^{-4}$  in the water extract is lower than that in the IEF extract (by a factor of 2.5), but is similar to that in groundwater samples from this site (17). A comparison of the chemical compositions of the original soil, the water extract, and the IEF extract is given in Table 1.

Hydrolyzable neutral sugars and uronic acids of this IEF extract are quite varied (Figure 1), with a xylose to mannose ratio around 0.3. This suggests a dominant contribution from plant debris and minor levels of carbohydrates from microbial degradation (18, 19). In addition, the ratio of neutral sugars to uronic acids, a value of 16, confirms this dominance of plant sugars, if it is assumed that uronic acids are mainly microbial oxidation products of neutral sugars (19).

**Elemental Mapping.** Elemental mapping obtained by synchrotron-based  $\mu$ -XRF displays a diffuse and homogeneous distribution of Fe in the IEF extract (Figure 2a, right), which is very different from the discrete iron oxyhydroxides associated with NOM that exist in the water extract (Figure 2a, left) (20). Elemental mapping for Ti (Figure 2b) and Mn (Figure 2c) shows results similar to that of iron. Calcium is evenly distributed throughout both the water extract and the IEF extract (Figure 2d). Cu, Cr, Ni, and Zn show results similar to that of Ca (images not shown). X-ray absorption near edge spectroscopy (XANES) analysis of the iron and manganese in the water extract performed at the K-absorption edge (7112 and 6539 eV, respectively), indicates that the iron in the colloid is present in the ferric form (Figure S4) and Mn as  $Mn^{4+}$  (images not shown). Though the Pu concentrations in both samples are below the detection limit of this method, the spatial distribution of other tetravalent elements, e.g.,  $Ti^{4+}$  and  $Mn^{4+}$ , closely matches that of iron. Very likely, the IEF extract contains homogeneously distributed organic functionalities that complex Fe(III), as well as other tetravalent ions (Ti and Mn), a pattern that is totally different from the previously identified inhomogeneously bound Pu-carrying amorphous Fe hydroxide pseudocolloid reported in groundwater (4). While one could argue that the resolution is not high enough (10  $\mu m$  pixel size) to make this statement, a thermodynamic assessment of the co-occurrence of small iron colloids and hydroxamate and other iron chelating functional groups (see below) strongly argues against such possibility (21), as these chelating ligands cause ligand-promoted dissolution. A similar argument can be made against the presence of plutonium oxyhydroxides (e.g., refs 22, 23, 24).

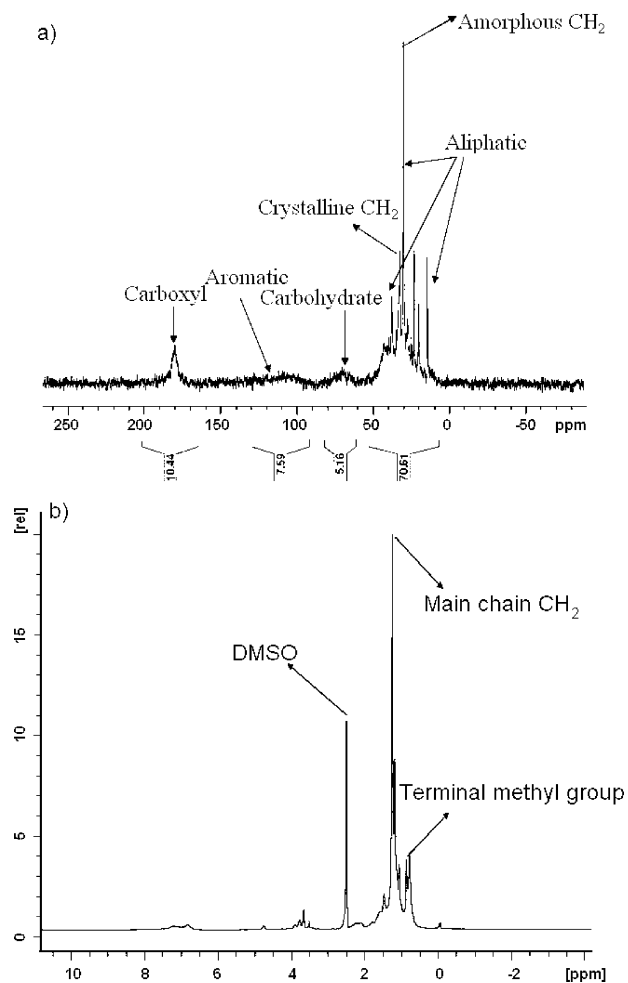
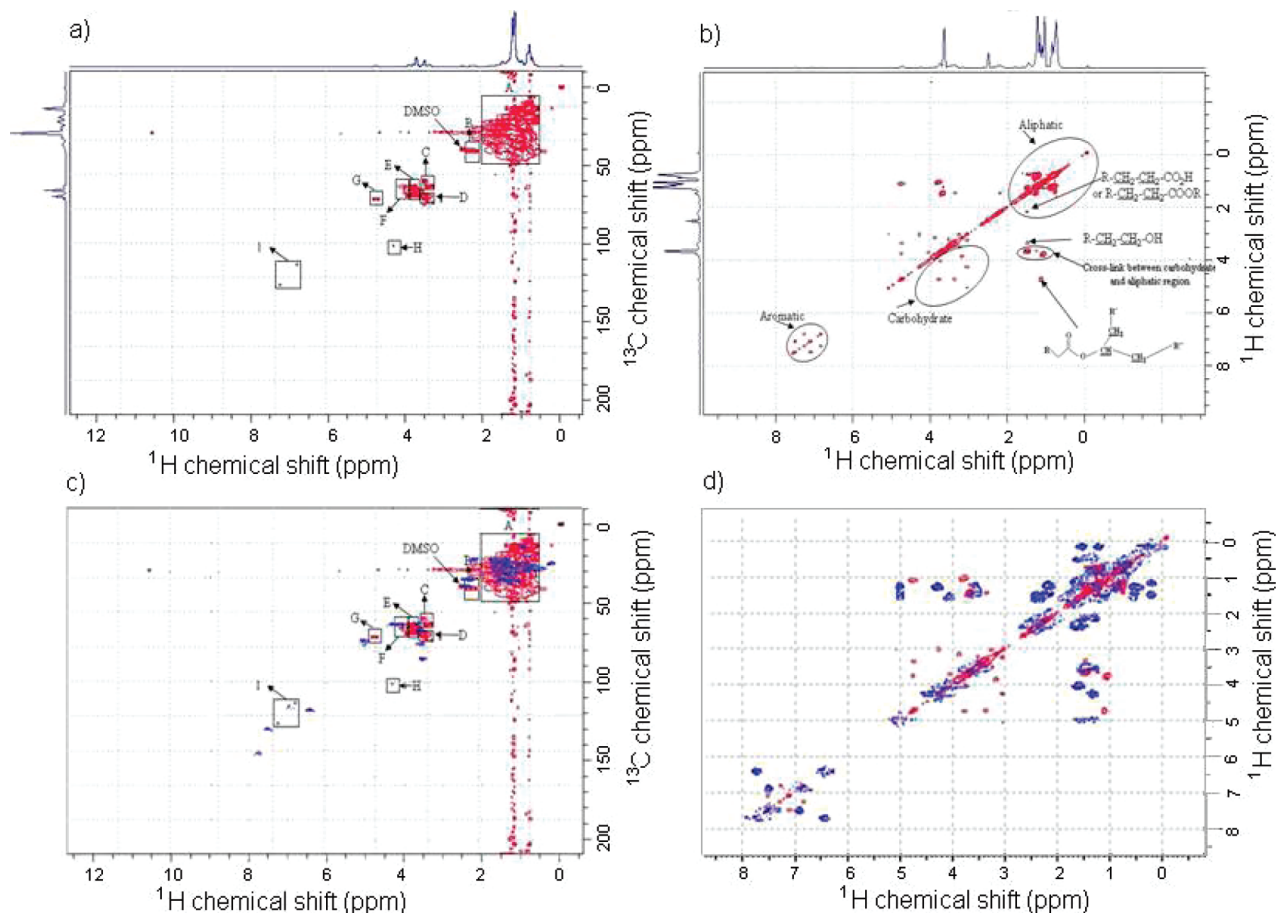


FIGURE 4. (a) Solid-state cross-polarization magic angle spinning (DPMAS)  $^{13}C$  NMR spectrum of RFETS soil IEF extract (the vertical numbers at the bottom indicate the normalized integrals) and (b) 1D  $^1H$  HRMAS NMR spectrum of RFETS soil IEF extract in  $DMSO-d_6$ .

**Functional Groups.** Functional groups of the IEF extract investigated by ATR-FTIR (Figure 3) show intense bands at 2920 and 2852  $cm^{-1}$  characteristic of saturated aliphatic C–H stretching. Very strong aliphatic C–H bending vibrations are



**FIGURE 5.** 2D NMR spectra of RFETS soil IEF extract swollen in DMSO- $d_6$ : (a) HSQC NMR spectrum; (b) COSY NMR spectrum; (c) overlapping of the HSQC NMR spectrum of the IEF extract (red), tomato cuticle (green) (30), and spectral simulations of the model cutin monomeric unit ((31), black; (32), blue); (d) overlapping of the COSY NMR spectrum of the IEF extract and spectral simulations of the model cutin monomeric unit ((31), black; (32), blue). The spectral assignments for the HSQC spectrum (a) of the IEF extract are the following: (1) terminal methyls and methylene groups in long-chain structures (box A); (2) methine structures attached to carbonyl groups in  $\alpha$ -methyl branched fatty acids and esters (box B); (3) methylene structures attached to hydroxyl groups (box C); (4) methylene structures attached to ether oxygens or methane groups attached to a secondary alcohol (box D); (5) CH groups in carbohydrates (box E); (6) methylene structures attached to the singly bonded oxygen of esters (box F); (7) methines attached to the singly bonded oxygen of esters (box G); (8) anomeric carbons in carbohydrates (box H); and (9) aromatic structures (box I).

also found at  $1455\text{ cm}^{-1}$ . Both support the presence of fatty acids or esters. The band at  $1724\text{ cm}^{-1}$  can be attributed to the stretching vibrations of carbonyl groups in fatty esters/fatty acids. A rather intense band for the amide I vibration ( $\text{C}=\text{O}$  stretching,  $1660\text{ cm}^{-1}$ ) is observed and a concomitant shoulder is observed for the amide II ( $\text{N}-\text{H}$  bending vibration and  $\text{CN}$  stretching vibration,  $1556\text{ cm}^{-1}$ ). These suggest the presence of amide or hydroxamate groups. A hump at  $3200\text{ cm}^{-1}$  might represent  $\text{NH}_2$  aminoacidic groups. The presence of sulfate is suggested by two groups of bands:  $1247\text{ cm}^{-1}$  ( $\text{S}=\text{O}$  stretching) and  $823\text{ cm}^{-1}$  ( $\text{C}-\text{O}-\text{S}$  stretching). Carboxylate groups are indicated by the  $\text{COO}^-$  asymmetric stretching vibration at  $1615\text{ cm}^{-1}$  as well as the symmetric stretching vibration around  $1400\text{--}1377\text{ cm}^{-1}$ . The presence of organic phosphate is indicated by two bands at  $1247\text{ cm}^{-1}$  and  $1218\text{ cm}^{-1}$ . However, the band around  $1250\text{ cm}^{-1}$  could also be related to the phenolic  $-\text{OH}$  groups. The band around  $1370\text{ cm}^{-1}$  can also be attributed to phenolic  $\text{C}-\text{OH}$  stretching. Except for the band around  $1660\text{ cm}^{-1}$ , which is usually attributed to the amide I, bands within the region of  $1500\text{--}1700\text{ cm}^{-1}$  can also be attributed to the  $\text{C}=\text{C}$  stretching of aromatic rings. Distinct bands at  $1083$  and  $1043\text{ cm}^{-1}$  are particularly characteristic of the  $\text{C}-\text{O}-\text{C}$  group vibrations of carbohydrates.

The main carbon functionalities are identified in the solid-state DPMAS  $^{13}\text{C}$  NMR (25) as consisting of carboxyl/amide

groups, aromatic rings, carbohydrates, and aliphatic chains (Figure 4a), and representing 10.44%, 7.59%, 5.16%, and 70.61% of OC, respectively, based on an integration of the individual spectra. Although the lipid and ester content was not independently determined in this study, the carbohydrate content matched well with the spectrophotometric analysis, i.e., 4.7% of OC. The aliphatic signal representing long-chain polymethylene carbons ( $\sim 29\text{ ppm}$ ) was dominantly composed of  $\text{CH}_2$  groups having amorphous character (made up of random cis/trans orientations). Polymethylene carbons having a crystalline character, the peak at  $\sim 32\text{ ppm}$  for  $\text{CH}_2$  units arranged in all trans configurations (26), is subordinate. Another important feature of the spectrum is the carboxyl/amide peak at  $180\text{ ppm}$ , whose chemical shift indicates the carboxyl or amide groups are clustered closely together, with the oxygen mainly complexed by metals (16), e.g., Fe. Problems like overlapping resonance lines, selective quenching intensity, and loss of signals (27) can be ignored due to the relatively low concentration of Fe (III) (Fe/C atom ratio of  $5 \times 10^{-4}$ , Table 1) in the IEF sample. In the 1D  $^1\text{H}$  HRMAS spectrum (Figure 4b), the peaks representing terminal methyl protons ( $\sim 1.0\text{ ppm}$ ) indicate that this isolate contains an abundance of terminal branching as a result of extensive diagenesis and, thus, the macromolecule has become more recalcitrant to biodegradation (28). Main-chain  $\text{CH}_2$  groups are identified in abundance at around  $1.3\text{ ppm}$ . Assignments

of other signals, indicated in Figure 4b, are made on the basis of the 2D HRMAS data.

Both HSQC (Figure 5a) and COSY (Figure 5b) NMR spectra indicate the presence of cross peaks that match those shown for cutin (29), and, thus, it is very likely that this IEF extract is cuticle-type material. Further support for this conclusion is provided by comparisons to previously identified cutin spectra (30) and spectral simulations (Figure 5c and d) of the cutin model structures (31, 32), respectively. The elevated N/C ratio in the IEF extract over that in the water extract is ascribed to the presence of abundant ester/amide groups and some amino acid groups observed by both ATR-FT/IR (Figure 3) and solid state  $^{15}\text{N}$  NMR (Figure S5), though the signal of the latter is weak due to the limited sample amount. Evidence of cross-linked structures like  $\alpha$ -branched fatty acids/esters (box B, Figure 5a) and esters of midchain hydroxyls (box G, Figure 5a) have been previously identified in cutin (33). The relatively low O-alkyl-C/alkyl-C ratio, the low abundance of aromatic groups and labile components (e.g., polysaccharides), as well as the high nitrogen content would suggest a highly recalcitrant and insoluble property of this substance (34). The high nitrogen content is of interest because cutin is usually devoid of nitrogen. It is possible that the nitrogen has been incorporated into cutin-like structures by processes yet to be defined.

Cutin is normally regarded as a water-insoluble macromolecule; this attribute appears to be inconsistent with the fact that this IEF isolate originates from a soil–water extract. It could be rationalized that it probably contains sufficient amounts of polar functional groups to induce solubility. The DPMAS spectrum shown in Figure 4a shows the presence of possible carboxyl or amide functionalities that could provide solubility. It is also possible that the isolate exists encapsulated or cross-linked within a hydrophobic domain of an otherwise hydrophilic moiety of colloidal organic matter, e.g., polysaccharides (Table 1 and Figure 1), that renders it soluble.

Siderophores produced by bacteria and fungi (35, 36) have been proposed as the strongest chelating agents for actinide elements as a result of multinuclear complexation at the carbonyl- or hydroxamate-oxygen, or amide-nitrogen, and their ability to dissolve oxyhydroxides of iron (21, 22), and, most importantly, also plutonium (23, 24). Though NMR analysis applied in this study did not directly show protons associated with the hydroxamate functionality, a high abundance of nitrogen, a strong amide functionality, and a low protein content in this IEF extract indicates the possible presence of hydroxamate, which is regarded as a typical functional group of siderophores. Quantitative determination of hydroxamate functional groups by a modified colorimetric Csaky test ((37); also see Supporting Information) showed that about 1.2% of the C is present as hydroxamate, with the IEF extract being enriched by a factor of 10 (% mass) and 2 (% OC) in hydroxamate, compared with the original bulk soil (Table 1). Since there are many siderophores that do not contain hydroxamate (e.g., rhizoferrin from soil fungi, which contains only carboxylates), the presence of even 1% hydroxamate suggests that siderophores decomposition products are important moieties in this mobile Pu-carrying biopolymer. Based on the chemical composition (Table 1), a stoichiometry of Fe/Carboxyl-C/N of close to 1:200:400 provides ample opportunities for chelating or clustered Fe (and Pu) binding sites. It is important to point out that the idea of siderophores as carriers of Pu and other actinides has never been tested in the field, where actinide (e.g., Pu or Th) concentrations are many orders of magnitude (e.g.,  $10^9$  to  $10^{12}$ ) lower than that in laboratory experiments (38), which makes it very difficult to probe the in situ binding environment of Pu.  $^{239,240}\text{Pu}/\text{Fe}$  ratios of (7 or 3)  $\times 10^6$  pCi Pu/g-Fe are observed in the water or IEF extracts, equivalent to  $^{239}\text{Pu}/\text{Fe}$  atomic ratios of (26 or 11)  $\times 10^{-6}$ , respectively, suggesting

that Pu would only have to substitute about one in  $10^5$  binding sites of Fe(III).

The negatively charged amphiphilic biopolymer that was isolated here has strong metal complexing ability, as well as surfactant and emulsifier qualities (3), giving it both high mobility in the surface environment and the ability to at least temporarily adhere to soil particles. Pu is likely complexed by a cutin-like substance containing hydroxamate, carboxylic, and amide chelating functional groups that are likely derived from siderophores, which in their pure state normally have a molecular weight of 500–700 Da. This newly characterized 6 kDa plutonium carrier likely contains degradation products of cutin, as the backbone, which is the hydrophobic waxy layer covering plant surfaces and must be abundant in this grassland area, cross-linked to a siderophore degradation product and hydrophilic carbohydrate moieties during microbial degradation. This cross-linking enhances both its complexation ability as well as its mobility, and makes it an ideal collector for actinides and other metals, and a vector for the dispersal of Pu.

### Acknowledgments

This work was supported by the Environmental Remediation Sciences Program, Environmental Remediation Sciences Division, Office of Biological and Environmental Research, Office of Science, Department of Energy, U.S. Department of Energy, Grant DE-FG02-04ER63899 and under Contract DE-AC02-98CH10886, and in part by the Texas Institute of Oceanography. We thank I.D. Ruhl (ODU) for help with NMR analysis and Dr. Aijun Miao (TAMUG) for help with GFAAS.

### Supporting Information Available

Details of the working conditions and parameters for IEF, NMR, Microsynchrotron X-ray fluorescence (SXRF) and  $\mu$ -X-ray absorption near edge structure ( $\mu$ -XANES) analysis. This material is available free of charge via the Internet at <http://pubs.acs.org>.

### Literature Cited

- 1) Kersting, A. B.; Efund, D. W.; Finnegan, D. L.; Rokop, D. J.; Smith, D. K.; Thompson, J. K. Migration of plutonium in groundwater at the Nevada Test Site. *Nature* **1999**, *397*, 56–59.
- 2) Dai, M. H.; Kelley, J. M.; Buesseler, K. O. Sources and migration of plutonium in groundwater at the Savannah River Site. *Environ. Sci. Technol.* **2002**, *36*, 3690–3699.
- 3) Santschi, P. H.; Roberts, K. A.; Guo, L. D. The organic nature of colloidal actinides transported in surface water environments. *Environ. Sci. Technol.* **2002**, *36*, 3711–3719.
- 4) Novikov, A. P.; Kalmykov, S. N.; Utsunomiya, S.; Ewing, R. C.; Horreard, F.; Merkulov, A.; Clark, S. B.; Tkachev, V. V.; Myasoedov, B. F. Colloid transport of plutonium in the far-field of the Mayak Production Association, Russia. *Science* **2006**, *314*, 638–641.
- 5) Boukhalfa, H.; Icopini, G. A.; Reilly, S. D.; Neu, M. P. Plutonium(IV) Reduction by the Metal-Reducing Bacteria *Geobacter metallireducens* GS15 and *Shewanella oneidensis* MR1. *Appl. Environ. Microbiol.* **2007**, *73*, 5897–5903.
- 6) Francis, A. J.; Dodge, C. J.; Ohnuki, T. Microbial transformations of plutonium. *J. Nucl. Radiochem. Sci.* **2007**, *8*, 121–126.
- 7) Choppin, G. R.; Morgenstern A. Distribution and movement of environmental plutonium. In *Plutonium in the Environment*; Kudo, A., Ed.; Elsevier Science Ltd.: New York, 2001; pp 91–105.
- 8) Runde, W. The chemical interactions of actinides in the environment. *Los Alamos Sci.* **2000**, *26*, 392–411.
- 9) Clark, D. L.; Janecky, D. R.; Lane, L. J. Science-based cleanup of Rocky Flats. *Phys. Today* **2006**, *59*, 34–40.
- 10) Hung, C. C.; Santschi, P. H. Spectrophotometric determination of total ionic acids in seawater using cation exchange separation and pre-concentration by lyophilization. *Anal. Chim. Acta* **2001**, *427*, 111–117.
- 11) Smith, P. K.; Krohn, R. I.; Hermanson, G. T.; Mallia, A. K.; Gartner, F. H.; Provenzano, M. D.; Fujimoto, E. K.; Goeke, N. M.; Olson, B. J.; Klenk, D. C. Measurement of protein using bicinchoninic acid. *Anal. Biochem.* **1985**, *150*, 76–85.

- (12) Solórzano, L.; Sharp, J. H. Determination of total dissolved phosphorus and particulate phosphorus in natural waters. *Limnol. Oceanogr.* **1980**, *25*, 754–758.
- (13) Guo, L.; Santschi, P. H. Isotopic and elemental characterization of colloidal organic matter from the Chesapeake Bay and Galveston Bay. *Mar. Chem.* **1997**, *59*, 1–15.
- (14) Grotjan, H. E., Jr.; Padrnos-Hicks, P. A.; Keel, B. A. Ion chromatographic method for the analysis of sulphate in complex carbohydrates. *J. Chromatogr.* **1986**, *367*, 367–375.
- (15) Walters, J. S.; Hedges, J. I. Simultaneous determination of uronic acids and aldoses in plankton, plant tissues, and sediment by capillary gas chromatography of N-hexylaldonamide and alditol acetates. *Anal. Chem.* **1988**, *60*, 988–994.
- (16) Leenheer, J. A.; Brown, G. K.; MacCarthy, P.; Cabaniss, S. E. Models of metal binding structures in fulvic acid from the Suwannee River, Georgia. *Environ. Sci. Technol.* **1998**, *32*, 2410–2416.
- (17) Roberts, K. A.; Santschi, P. H.; Leppard, G. G.; West, M. Characterization of organic-rich colloids from surface and ground waters at the actinide-contaminated Rocky Flats Environmental Technology Site (RFETS), Colorado, USA. *Colloids Surf., A* **2004**, *244*, 105–111.
- (18) Murata, T.; Nagaishi, N.; Hamada, R.; Tanaka, H.; Sakagami, K.; Kato, T. Relationship between soil neutral sugar composition and the amount of labile soil organic matter in Andisol treated with bark compost or leaf litter. *Biol. Fertil. Soils* **1998**, *27*, 342–348.
- (19) Fischer, H.; Meyer, A.; Fischer, K.; Kuzyakov, Y. Carbohydrate and amino acid composition of dissolved organic matter leached from soil. *Soil Biol. Biochem.* **2007**, *39*, 2926–2935.
- (20) Ablett, J.; Kao, C.; Reeder, R.; Tang, Y.; Lanzirrotti, A. X27A—a new hard X-ray micro-spectroscopy facility at the national synchrotron light source. *Nucl. Instrum. Meth. A* **2006**, *562*, 487–494.
- (21) Holmen, B. A.; Casey, W. H. Hydroxamate ligands, surface chemistry, and the mechanism of ligand promoted dissolution of goethite (alpha-FeOOH(s)). *Geochim. Cosmochim. Acta* **1996**, *60*, 4403–4416.
- (22) Brainard, J. R.; Strietelmeier, B. A.; Smith, P. H.; Langston-Unkefer, P. J.; Barr, M. E.; Ryan, R. R. Actinide binding and solubilization by microbial siderophores. *Radiochim. Acta* **1992**, *58/59*, 357–363.
- (23) Ruggiero, C. E.; Matonic, J. H.; Reilly, S. D.; Neu, M. P. Dissolution of plutonium(IV) hydroxide by desferrioxamine siderophores and simple organic chelators. *Inorg. Chem.* **2002**, *41*, 3593–3595.
- (24) Whisenhunt, D. W., Jr.; Neu, M. P.; Hou, Z.; Xu, J.; Hoffman, D. C.; Raymond, K. N. Specific Sequestering Agents for the Actinides. 29. Stability of the Thorium(IV) Complexes of Desferrioxamine B (DFO) and Three Octadentate Catecholate or Hydroxypyridinone DFO Derivatives: DFOMTA, DFO-CAMC, and DFO-1,2-HOPO. Comparative stability of the plutonium(IV) DFOMTA complex. *Inorg. Chem.* **1996**, *35*, 4128–4136.
- (25) Simpson, A. J.; Song, G.; Smith, E.; Lam, B.; Novotny, E. H.; Hayes, M. H. B. Unraveling the structural components of soil humin by use of solution-state nuclear magnetic resonance spectroscopy. *Environ. Sci. Technol.* **2007**, *41*, 876–883.
- (26) Hu, W. G.; Mao, J. D.; Xing, B. S.; Schmidt-rohr, K. Poly(methylene) crystallites in humic substances detected by nuclear magnetic resonance. *Environ. Sci. Technol.* **2000**, *34*, 530–534.
- (27) Preston, C. M.; Newman, R. H.; Rother, P. Using <sup>13</sup>C CPMAS NMR to assess effects of cultivation on the organic matter of particle size fractions in a grassland soil. *Soil Sci.* **1994**, *157*, 26–35.
- (28) Schaeffer, T. L.; Cantwell, S. G.; Brown, J. L.; Watt, D. S.; Fall, R. R. Microbial growth on hydrocarbons: terminal branching inhibits biodegradation. *Appl. Environ. Microbiol.* **1979**, *38*, 742–746.
- (29) Deshmukh, A. P.; Simpson, A. J.; Hadad, C. M.; Hatcher, P. G. Insights into the structure of cutin and cutan from *Agave americana* leaf cuticle using HRMAS NMR spectroscopy. *Org. Geochem.* **2005**, *36*, 1072–1085.
- (30) Kelleher, B. P.; Simpson, A. J. Humic substances in soils: are they really chemically distinct? *Environ. Sci. Technol.* **2006**, *40*, 4605–4611.
- (31) Fang, X.; Qiu, F.; Yan, B.; Wang, H.; Mort, A. J.; Stark, R. E. NMR studies of molecular structure in fruit cuticle polyesters. *Phytochemistry* **2001**, *57*, 1035–1042.
- (32) Kolattukudy, P. E. Polyesters in higher plants. *Adv. Biochem. Eng./Biotechnol.* **2001**, *71*, 1–49.
- (33) Deshmukh, A. P.; Simpson, A. J.; Hatcher, P. G. Evidence for cross-linking in tomato cutin using HR-MAS NMR spectroscopy. *Phytochemistry* **2003**, *64*, 1163–1170.
- (34) Mathers, N. J.; Jalota, R. K.; Dalal, R. C.; Boyd, S. E. <sup>13</sup>C-NMR analysis of decomposing litter and fine roots in the semi-arid Mulga Lands of southern Queensland. *Soil Biol. Biochem.* **2007**, *39*, 993–1006.
- (35) Neilands, J. B.; Leong, S. A. Siderophores in relation to plant growth and disease. *Ann. Rev. Plant Physiol.* **1986**, *37*, 187–208.
- (36) Renshaw, J. C.; Robson, G. D.; Trinci, A. P. J.; Wiebe, M. G.; Livens, F. R.; Collison, D.; Taylor, R. J. Fungal siderophores: structures, functions, and applications. *Mycological Res.* **2002**, *106* (10), 1123–1142.
- (37) Gillam, A. H.; Lewis, A. G.; Anderson, R. J. Quantitative determination of hydroxamic acids. *Anal. Chem.* **1981**, *53*, 841–844.
- (38) Boukhalfa, H.; Reilly, S. D.; Neu, M. P. Complexation of Pu(IV) with the natural siderophore desferrioxamine B and the redox properties of Pu(IV)(siderophore) complexes. *Inorg. Chem.* **2007**, *46*, 1018–1026.

ES801348T